A Linear Analysis of the Multiple Vortex Phenomenon in Simulated Tornadoes

ROBERT L. GALL

Institute of Atmospheric Physics, The University of Arizona, Tucson 85721

(Manuscript received 7 December 1982, in final form 25 April 1983)

ABSTRACT

A simple vertically-integrated axisymmetric model is used to calculate axisymmetric flows for different swirl ratios (S) in tornado simulators. These axisymmetric states are then tested for stability using a primitive-equation linear model where the waves have both an azimuthal and a vertical wavenumber.

For S high enough for there to be a central downdraft in the axisymmetric vortex, the vortex is unstable; otherwise it is stable. For relatively low S, only azimuthal waves 1 and 2 are unstable, with wave 1 most unstable at low S, followed by 2 at somewhat higher S. As S is further increased, the most unstable wave shifts to 4, then 5, and so forth. With some tuning, the model predicts the transitions from 0–1 and 1–2 secondary vortices to occur at about the observed value of S. Vertical wavelengths are about 3 m, but they increase with increasing S.

There are two modes of instability: one in which only waves 1 or 2 are unstable and which appears at low S, and a second mode where waves 4, 5 or 6 are most unstable and which appears at high S. These two modes are distinguished mostly by their energetics. Mode 1 receives most of its energy from the radial shear of the vertical wind, while mode 2 receives most of its energy from the radial shear of the tangential wind. In mode 1, all the amplitude of the horizontal streamfunction is contained inside the tangential wind maximum, while in mode 2 much of the amplitude is outside the tangential wind maximum.

1. Introduction

The existence of secondary vortices (also called suction spots) within the main circulation of a tornado has been described by a number of authors (e.g., Fujita, 1970; Agee *et al.*, 1977). It has been shown (e.g., Fujita, 1970) that much of the damage in large tornado events can be attributed to these secondary vortices. In other words, the damage within a large tornado track is greatest along cycloidal streaks within the track, presumably along the lines followed by the secondary vortices. The picture that emerges from the study of these damage tracks is that the secondary vortices have diameters considerably less than the diameter of the parent tornado, rotate about the center of the parent tornado at some common radius, and have wind velocities considerably higher than the maximum azimuthally averaged velocities. This picture of the secondary vortices has been confirmed through photographs of tornadoes where the multiple vortices were actually visible (Agee *et al.*, 1977).

It was the ability to simulate the secondary vortices, also known as the multiple-vortex phenomenon, in the laboratory that has provided us with our best quantitative picture of the secondary vortices. The first machine capable of simulating the secondary vortices was described by Ward (1972). This machine consisted of a vertical cylinder ~1.5 m tall and 2 m in diameter, with a fan-and-baffle arrangement at the top to draw air upward through the cylinder. Air enters the cylinder horizontally at the bottom through a rotating screen. Thus the fan provides an updraft, and hence a converging layer of air at the bottom of the chamber, while the rotating screen provides angular momentum to the converging layer. Great care is taken to assure that the properties of the incoming air are axisymmetric. A thorough discussion of this type of machine is available in Ward (1972) and Church *et al.* (1979). See Figs. 1 and 2 of Church *et al.* (1979) for diagrams illustrating the apparatus.

The flow that develops in the machine is primarily a function of the swirl ratio

$$S = \frac{\Gamma r_0}{Q},$$

where Γ is the circulation at r_0, the radius of the outer edge of the apparatus, and Q is the volume flow rate. At low swirl ratio (for fixed Q, this would imply a relatively low rotation rate for the screen), there is a single very narrow laminar vortex in the center of the chamber. With increasing swirl ratio, the vortex widens and becomes turbulent (probably due to an internal instability) with a dynamically induced downdraft eventually developing along the center line of the chamber. At values of S between 0.5 and 1.0, secondary vortices appear at some radius away from the center: first, one spiraling around the center line, then two followed by three, and so forth, as the swirl ratio increases. The radius at which the secondary vortices are found also increases with increasing swirl.

A thorough discussion of the vortices that appear in the machine is available in Church *et al.* (1979). The remarkable similarity between the simulated vortices and natural vortices, such as tornadoes and dust devils, is discussed in Church and Snow (1979).

Because the forcing of the flow in the tornado simulator is very close to axisymmetric, the development of the secondary vortices, which must be viewed as axi-asymmetries, cannot be explained by any external forcing mechanism. They must be due to an internal instability. It has been discussed by others (Ward, 1972; Church *et al.*, 1979; Rotunno, 1977) that regions of strong horizontal shear exist in the wind field surrounding the vortex; and, in fact, when a downdraft is present along the center line of the vortex, most of the vorticity of the system is contained in a narrow annular ring. Thus a barotropic or shear instability is suggested. (Since there are no temperature gradients in the apparatus, a baroclinic instability is clearly eliminated.)

A thorough analysis of the dynamic stability of the vortex in the tornado simulator has not yet appeared in the literature, although there have been some preliminary studies. Staley and Gall (1979) studied the barotropic instability (assuming that the secondary vortices were vertical and that there was no vertical wind in the basic state) of observed wind profiles in a tornado. Snow (1978) studied the inertial instability of hypothetical wind distributions in the simulator. Neither of these studies allowed for a vertical wind in the basic state, and neither used wind profiles that were solutions of the governing equations. Both showed that instability of the azimuthal wind could account for the presence of the secondary vortices, since the unstable vortices had growth rates that were large compared to the lifetime of the basic vortex. Rotunno (1978) included the radial shear of the vertical wind and found that inclusion of this shear caused the unstable waves to take on a spiral structure, unlike the waves in Staley and Gall, and in Snow. He also did not use basic states that were solutions to the governing equations. In fact, the vorticity sheets in his study were of infinitesimal thickness, which caused his most unstable azimuthal wavenumber to be infinite. More recently Rotunno (1982) has shown that the multiple vortex phenomenon can be simulated numerically using a three-dimensional model.

In this study we will use the axisymmetric model described by Gall (1982, hereafter referred to as G) to generate a series of basic states for various swirl ratios in the vortex simulator of Church *et al.* (1979). Fig. 1 illustrates the geometry of this simulator, where, for the experiment described later, r_0 (the radius of the updraft hole) is 62 cm, the depth d of the convergence zone is 42 cm, and the height of the convective region ($H - d$) is 166 cm. The axisymmetric model is thoroughly described in G. The flow

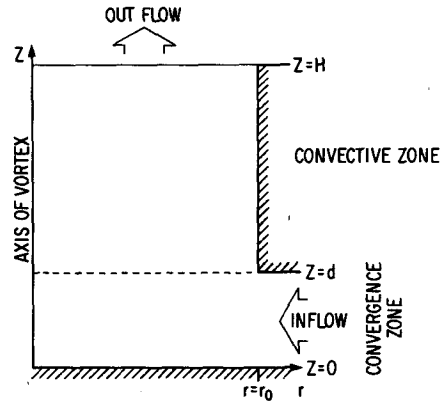

FIG. 1. Schematic illustration of the geometry of the tornado simulator. The axis of the vortex is assumed to be at the center of the cylindrical chamber. Hatched lines denote solid surfaces. At a large radius beyond $r = r_0$, the inflowing air passes through a screen which has been set to rotate about the center axis.

from the convective region of that model will be introduced into a primitive-equation linear model and tested for stability. In the stability analysis, the basic state will be assumed to be of infinite extent in the vertical. This assumption is necessary, since to keep this study relatively simple, we choose to describe the vertical variations of the secondary vortex with a vertical wavenumber. This assumption will be relaxed in subsequent studies where detailed structures in the vertical and upper and lower boundaries are retained. This assumption is justified here, since we suspect that the basic dynamics of the secondary vortices do not depend on these boundaries nor on the vertical variations of the basic state.

This linear analysis will allow a thorough discussion of the structure, energetics, and ultimately the source of the secondary vortices in the vortex simulator, at least from the point of view of the linearized equations.

2. Discussion

Before we proceed with discussion of the linear model and the stability analysis, some preliminary comments are necessary. Fig. 2 shows the vertical and azimuthal components of vorticity from the convective region of the axisymmetric model for a swirl ratio of 1.0 and eddy viscosity in the axisymmetric model of $K = 1.5$ cm^2 s^{-2} and $K = 6$ cm^2 s^{-2}. All other parameters necessary to specify the experiment are the same as in G (i.e., the volume flow rate was 0.708 m^2 s^{-1}, and F, a parameter used in the model in G, was 0.75).

In the experiments described in G, a value of $K = 1.5$ was used. Note that for this value of K, the vorticities are confined to a very narrow sheet and that the maximum vertical vorticity greatly exceeds the maximum magnitude of the azimuthal vorticity.

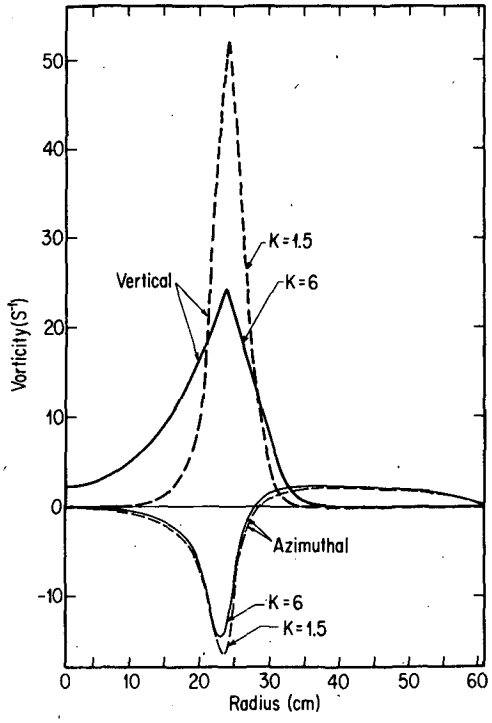

FIG. 2. Radial distribution of the vertical and azimuthal components of vorticity from the axisymmetric model of Gall (1982) for two different values of the mixing coefficient K ($cm^2\ s^{-1}$) used in that model.

Intuitively, we might expect that the instability of the basic vortex is due to the presence of these vorticity sheets and that the relative importance of the vertical vorticity to the azimuthal vorticity in the instability should be determined by the ratio of their maximum magnitude. Thus when $K = 1.5$ at a swirl ratio of 1.0 in G's model, we might expect that the role of the radial shear of the azimuthal wind would dominate the role of the radial shear of the vertical wind in determining the structure of the unstable waves. Indeed this was verified in subsequent stability studies. However, it is clear from observations of multiple vortices in the simulator that the azimuthal vorticity must play an important role, especially at a swirl ratio of 1.0 [This is shown by the spiral nature of the vortices (Rotunno, 1977).]

In G no attempt was made to vary K; however, K is in fact one means by which the linear stability of the axisymmetric model can be tuned. A value of $K = 1.5$ probably represents a relatively low level of turbulence, which is certainly the case at low swirl ratios when the core is laminar. However, at swirl ratios where a downdraft is present the flow is turbulent, suggesting that a higher value of K should be employed at those swirl ratios. It is not known what value of K is most appropriate at any swirl ratio; however, a higher value of K than was used in G could perhaps be justified at values of S where there is a downdraft in the axisymmetric solution. Also shown in Fig. 1 are the vorticity distributions in the axisymmetric model when $K = 6$. Note that now the magnitude of the vertical vorticity is comparable to the magnitude of the azimuthal vorticity. Subsequent stability analysis of this profile showed that the role of radial shear of the vertical wind does strongly influence the wave structure since, for this profile, the vertical wavelength of the unstable disturbance is ~3–4 m. Further increase in K would, in fact, further increase the role of the azimuthal vorticity in the instability. However, after $K = 6$, a doubling of K only slightly changes the relative magnitudes of the two vorticities. Since $K > 10$ would be a rather large mixing coefficient, we arbitrarily selected $K = 6$ as a good compromise between a very large value of K and realistic linear results. Thus most subsequent calculations used this value of K. The mixing coefficient in the linear model allows further tuning of the results, as is discussed in Section 4.

Fig. 3 shows the growth rate spectrum at various swirl ratios calculated using the linear, inviscid, nondivergent barotropic model described by Staley and Gall (1979), which will be referred to as the nondivergent model. In that model, only the azimuthal wind of the basic state is used and the perturbations are independent of height.[1] We present these results here because they represent a standard to which the more complete results may be compared, and they can be used to illustrate an important point.

First note that, for swirl ratios less than 0.4, when $K = 6$ is used in the axisymmetric model, the nondivergent model implies the vortex is stable. For S less than 0.4, there is an updraft at the center of the axisymmetric vortex, and all the vertical vorticity of the system is contained in a narrow core at the center of the chamber. At $S > 0.4$ in the axisymmetric model, there is a downdraft at the center, and the vertical vorticity is now in the annular ring. This latter configuration of vorticity satisfies the usual necessary condition for barotropic instability. For $S < 0.4$, the necessary condition is not satisfied. Thus it is not surprising to find stability at $S < 0.4$. At $S > 0.4$, wave 2 is most unstable. At $S > 1.5$, the maximum instability shifts abruptly to wave 4 or 5, and at $S > 4.5$, wave 5 is most unstable. Note that most of

[1] We prefer to use the term nondivergent barotropic model (where we mean horizontal divergence) or simply nondivergent model, to refer to this model simply for convenience. Since there are no temperature gradients within the simulator, even the full model, to be described later, is clearly barotropic; hence, any instability associated with this model is itself a barotropic instability. Indeed it is probable that those instabilities themselves are nondivergent in an appropriate coordinate system (i.e., one where "horizontal" is orthogonal to the axis of the secondary vortex). However, such a coordinate system is conceptually rather cumbersome, and, if we retain the usual coordinate system in the full model, as we will, horizontal divergence is generally nonzero.

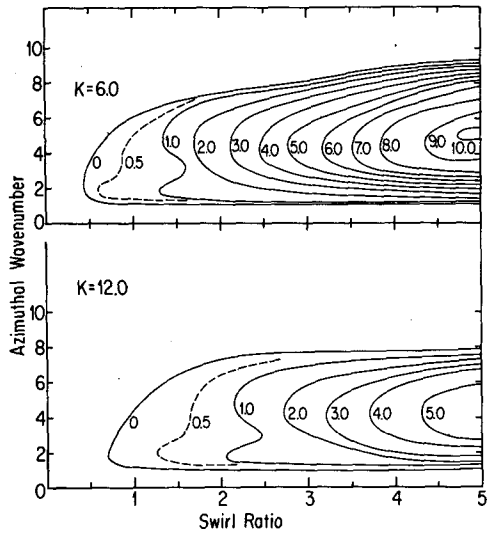

FIG. 3. Inviscid growth rates (s^{-1}) as a function of swirl ratio and azimuthal wavenumber for the tangential wind profiles from the axisymmetric model for two different values of the mixing coefficient K ($cm^2\ s^{-1}$) used in that model. The growth rates were calculated with the barotropic model described by Staley and Gall (1979).

the growth rates shown in Fig. 2 are quite large, indicating that the vortex is very unstable. An examination of the wave structure reveals that wave 2 at $S < 2$ is a different mode (hereafter called mode 1) than the most unstable mode at other wavenumbers and swirl ratios (mode 2). The abrupt shift in the most unstable wavenumber at $S = 1.5$ occurs because the instability of the second mode, which is less than that of the first mode at low S, increases more rapidly with S as compared to the instability of mode 1, and this second mode is most unstable at higher wavenumbers.

The lower part of Fig. 3 illustrates an important aspect of the linear dynamics that we feel explains the variation of the growth rate with S, shown in this figure and in Fig. 5. It also clearly shows how K can be used to tune the model. The bottom half of this figure is the same as the upper half, except $K = 12$ was used to produce the axisymmetric basic states. Note that the two figures are essentially the same except that, at any given swirl ratio, the growth rate for all wavenumbers is less when $K = 12.0$ and, in fact, the contours have all moved to the right with respect to the upper figure. Thus, the transitions from wave 2 to wave 4 and then 5, being most unstable, occur at higher swirl ratios.

The reduction in growth rates when K is increased is easily explained by the reduction in magnitude of the maximum of the vertical vorticity. In other words, as the vorticity in the annulus goes to zero, we would expect the instability to go to zero as well. Therefore, decreasing the magnitude of the vorticity sheet should decrease the instability. Since increasing K decreases the maximum vertical vorticity (see Fig. 2), the reduced growth rates when $K = 12$ are explained. The increase in the swirl ratio, where the most unstable wave shifts wavenumber, is somewhat more difficult to explain. We suspect that it is due to the fact that, as K is increased, the width of the annulus of vertical vorticity in the axisymmetric model also increases (i.e., increased diffusion spreads it out). For example, suppose that the most unstable wave will be the one that is most nearly circular and that the radial width of the most unstable wave is determined by the width of the ring of vorticity, i.e., the width of the unstable region. Since at a given swirl ratio, the radius of the ring of vorticity is unchanged but its width increases as K increases (see Fig. 1), then the *wavelength* of the most unstable mode would also increase with K if these waves are to remain more or less circular, and hence the most unstable wave should shift to lower wavenumbers.

Evidence that there is a relation between the width of the unstable region and the wavelength of maximum instability can be obtained by examining the traditional barotropic instability problem. If the ring of vorticity that we are discussing were at very large radius, then the flow could be described by the relation

$$U = U_0 \tan\left(\frac{y}{y_0}\right), \tag{1}$$

where y is a direction normal to the flow U. This particular profile was studied in some detail by Kuo (1973), and a discussion of its stability properties can be found in Haltiner and Williams (1980). In that study, we must take β (the variation of the Coriolis parameter with latitude) to be zero, if we wish an analogy with the present problem. When we do this it shows that, for this profile,

$$\frac{2\pi}{L} y_0 = 0.45 \text{ m}, \tag{2}$$

where L is the wavelength of the most unstable disturbance and y_0 is the parameter that controls the width of the shear zone. If we take the diameter D of the unstable disturbance to be half a wavelength (since a full wavelength includes both the positive and negative perturbations), then we can write

$$D \approx 7y_0. \tag{3}$$

Furthermore, if we take the width w of the shear zone to be $5y_0$ (this is of course arbitrary but seems reasonable, since it includes almost all of the shear), then

$$D \approx 1.4w. \tag{4}$$

Therefore, at least in the limit as the radius gets large, there is a strong relation between the width of the shear or unstable zone and the wavelength of maxi-

mum instability, in such a way that the most unstable vortices have a diameter nearly equal to the width of the shear zone.

A similar but simpler version of this problem was studied by Rayleigh (1880). He assumed that the vorticity was constant within a sheet of thickness w^*, and zero elsewhere. He showed that the most unstable wave had a wavelength about eight times the width of the vorticity sheet or, in terms of the notation above, $D \cong 4w^*$. Thus, in the limit, as the ring of vorticity goes to large radius, as the width of the ring increases, the wavelength of the maximum instability should increase.

We will not prove here that this result also applies for the strongly curved flow found in this problem. However, there is no reason to believe that this result will not hold at small radius.

This result also explains why the most unstable wavenumber increases with increasing S. As S increases, the radius of the maximum vorticity of the basic state increases, yet the width of the vorticity ring does not (see Fig. 6 of G). This is because this width is determined mostly by K, which is constant, while the radius is independent of K but depends on S. To be specific, note that the steady-state vertical vorticity distribution in the axisymmetric model is a balance between advective processes and diffusive processes [Eq. (17) of G]. If K were zero, all the vertical vorticity could be contained in an infinitesimal sheet at the radius where the radial velocity changes sign. With nonzero K, this sheet spreads out to a finite thickness, and this thickness must depend primarily on K. The radius where the radial velocity changes sign, of course, is a strong function of S. (See the discussion in G.) Thus, as the radius of the vorticity ring increases with increasing S, the *wavelength* of the most unstable mode stays unchanged; hence the *wavenumber* must increase.

These ideas are very similar to those expressed by Rotunno (1977) in his discussion section. He also speculates that the vertical wavelength will be determined by the thickness of the unstable region.

3. The linear model

What we will refer to as the full linear model is simply the linearized, incompressible primitive equations applied to a basic state (axisymmetric) vortex of infinite extent. Since the vortex is infinite, there can be no axisymmetric radial flow $\bar{V}_r$; hence the axisymmetric vertical velocity $\bar{W}$ and azimuthal velocity $\bar{V}_\theta$ are independent of height. Because of the above assumptions, the linear perturbations can be taken as periodic in the azimuthal θ direction and the vertical z direction. The basic states used in the calculations are the axisymmetric fields computed by the model given in G. The fields of $\bar{W}$ and $\bar{V}_\theta$ assumed to apply in the convective region of G's model are used. A discussion of these fields and their variation with swirl ratio is available in G.

Because G's model provides fields of $\bar{\delta}$ and $\bar{\xi}$ (the horizontal divergence and vertical vorticity, respectively), it was convenient to use the horizontal divergence and vertical vorticity equations for the linear model. The incompressible forms of the linearized vorticity and divergence equations are

$$\frac{\partial \xi'}{\partial t} = -V'_{r_\psi}\frac{\partial \bar{\xi}}{\partial r} - \bar{V}_{\theta_\psi}\frac{\partial \xi'}{\partial \theta} - \frac{1}{r}\frac{\partial}{\partial r}(r\bar{\xi}V'_{r_\chi}) - \frac{1}{r}\frac{\partial}{\partial \theta}(\bar{\xi}V'_{\theta_\chi}) + K_p\nabla^2\xi' + K_p\frac{\partial^2\xi'}{\partial z^2} - \frac{\partial \bar{W}}{\partial r}\frac{\partial V'_\theta}{\partial z} - \bar{W}\frac{\partial \xi'}{\partial z}, \quad (5)$$

$$\frac{\partial \delta'}{\partial t} = -\bar{V}_{\theta_\psi}\frac{\partial \delta'}{\partial \theta} + K_p\nabla^2\delta' + K_p\frac{\partial^2\delta'}{\partial z^2} + \frac{\partial \bar{W}}{\partial r}\frac{\partial V'_r}{\partial z} - \bar{W}\frac{\partial \delta'}{\partial z} + \frac{\partial^2\phi'}{\partial z^2}, \quad (6)$$

where the overbar denotes the basic state from the axisymmetric model and the prime indicates a deviation from this state; r is radius, positive outward; θ is angular position, positive counterclockwise; and K_p is the eddy viscosity for the perturbations. Also,

$$\delta' = -\frac{\partial W'}{\partial z}, \quad (7)$$

which is the incompressible continuity equation, and

$$\left.\begin{aligned}\xi' &= \nabla^2\psi'\\ \delta' &= -\nabla^2\chi\end{aligned}\right\}, \quad (8)$$

with similar relations for the basic state. The subscript ψ denotes the rotational part of the wind computed from the streamfunction ψ, and the subscript χ denotes the divergent part of the wind computed from the velocity potential χ. If neither χ nor ψ appears as a subscript, the total velocity is implied. ∇^2 is the horizontal Laplacian.

We define ϕ' as the perturbation pressure divided by density; it is computed from the three-dimensional, incompressible divergence equation

$$\nabla^2\phi' + \frac{\partial^2\phi'}{\partial z^2} = -\frac{2}{r}\frac{\partial V'_r}{\partial \theta}\frac{\partial \bar{V}_\theta}{\partial r} + \frac{2}{r}\frac{\partial}{\partial r}V'_\theta\bar{V}_\theta - \frac{\bar{V}_\theta}{r^2}\frac{\partial V'_r}{\partial \theta} - 2\frac{\partial \bar{W}}{\partial r}\frac{\partial V'_r}{\partial z}. \quad (9)$$

Boundary conditions are that the perturbation quantities vanish at the radius r_0.

Solutions to (5), (6) and (9) are obtained by first substituting, for example,

$$V'(\theta, r, z, t) = \tilde{V}(r, t)e^{i(k\theta+mz)}, \quad (10)$$

then replacing the radial and time derivatives by finite differences. For a specified k and m and for a given basic state, the model can be integrated in time from

an arbitrary initial perturbation. If after say 1000–2000 iterations, exponential growth of the perturbations is observed, we then say that the basic state is unstable. At that time, the most unstable mode dominates the perturbation; therefore, the structure of the most unstable mode is obtained. Growth rates and phase speeds of this mode can be computed directly from the perturbation quantities (e.g., see Brown, 1969). If after 2000 iterations growth is not exponential but rather the perturbation amplitudes are decaying with time, we say the basic state is stable.

4. The growth rate spectra

Just as the value of the friction coefficient used in the axisymmetric model can play a role in the stability of the basic vortex, so does the viscosity coefficient for the perturbations (K_p) used in the full linear model. It would seem obvious that one should pick the same value of this coefficient for both the axisymmetric flow and the perturbations, and this was done for most subsequent analyses. Fig. 3, however, illustrates that the choice of K_p can strongly affect the linear growth rate spectrum for a given basic state. Fig. 4 shows the growth rate spectrum for various azimuthal wavenumbers and vertical wavelengths for perturbations that spiral upward in a direction opposite to the rotation of the basic vortex. In both panels, $K = 6$ was used in the axisymmetric model, and the swirl ratio was 1.0. In the upper panel, K_p was 0; while in the lower panel it was 3. Similar results for $K_p = 6$ are given in Fig. 5. Note that for $K_p = 0$, the maximum growth is quite large and occurs for azimuthal wavenumber 5, vertical wavelength ~125 cm. Furthermore, no high-wavenumber cutoff in the instability was observed, at least up to azimuthal wavenumber 9. On introducing some friction, the growth rates are greatly reduced, and there are now two maxima of equal strength: one at azimuthal wavenumber 5 and vertical wavelength 150 cm, and a second at azimuthal wavenumber 2 and vertical wavelength ~500 cm. We will show later that these two regions represent two different modes of instability. Above wavenumber 7, the waves are stable. With $K_p = 6$, the two modes separate on the diagram, with one mode centered at azimuthal wavenumber 4, vertical wavelength 125 cm, and a second more unstable mode at wave 2, vertical wavelength 400 cm. $K_p = 6$ was chosen for the subsequent stability analysis primarily because, at a swirl ratio of 1.0 in the tornado simulator, two secondary vortices are observed.

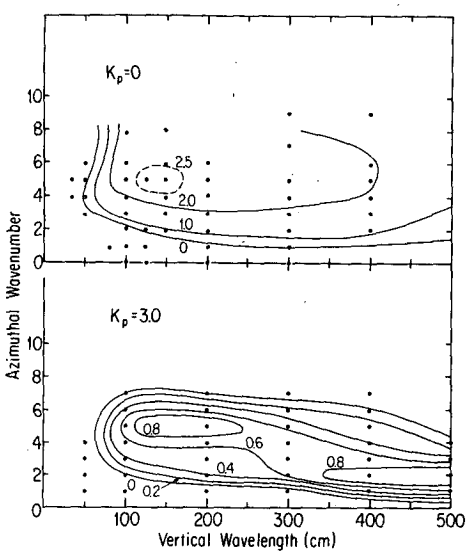

FIG. 4. Growth rates (s^{-1}) as a function of vertical wavelength and azimuthal wavenumber for two different values of the mixing coefficient K_p ($cm^2\ s^{-1}$) used in the full linear model. The basic state was taken from the axisymmetric model, which used a mixing coefficient $K = 6.0\ cm^2\ s^{-1}$ at a swirl ratio of 1.0. The dots denote points where the linear calculations were made. A growth rate of zero means that the perturbation was not growing or was damped.

As stated above, these as well as all subsequent results are for vortices with phase lines that at a given radius spiral upward in a direction opposite to the rotation of the basic vortex. If we take perturbations with the opposite spiral (i.e., by changing, for example, the sign of the vertical wavenumber) so that they spiral in the same direction as the rotation of the basic vortex, the vortex is still found to be unstable; however, when $K_p = 0$ the growth rates are less than half those shown in the upper part of Fig. 4. This was not surprising, since we might expect that the most unstable vortex would be more or less parallel to the total vorticity vector of the basic vortex (Rotunno, 1982; Maslowe, 1974), which in the region of maximum vertical vorticity has a component opposite to the rotation of the basic vortex.

It is also not surprising that the basic vortex is unstable to vortices that spiral in opposite directions but have the same vertical and azimuthal wavenumber, since in the limit as the vertical velocity goes to zero, the growth rates of these two vortices become the same. We don't expect the vertical velocity to eliminate an instability, only to modify it.

The growth rate spectra for $K = 6$ and $K_p = 6$ at other swirl ratios are given in Fig. 5. At $S = 0.4$ (not shown), all waves are stable. At that swirl ratio, however, the vertical velocity in the basic vortex is everywhere upward, and the vertical vorticity is confined to the center. By $S = 0.5$, a downdraft has appeared at the center of the basic vortex, the vertical vorticity of the system is in an annular ring about the center, and the vortex is unstable. Fig. 5 shows the growth rate spectrum at $S = 0.6$ and shows that both waves 1 and 2 are unstable, with wave 1 more unstable than 2 and most unstable at a vertical wavelength of 350 cm. The figure for $S = 0.5$ looks the same as for $S = 0.6$, and is therefore not shown.

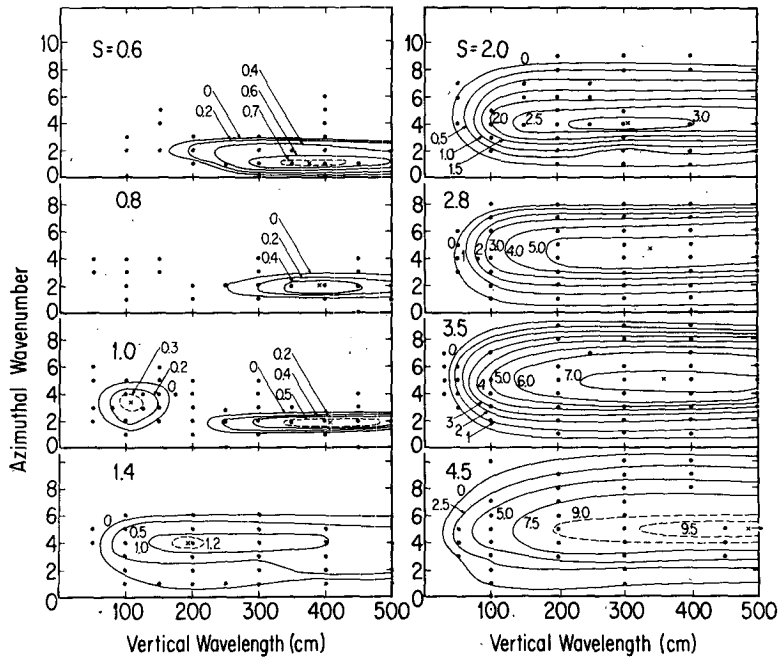

FIG. 5. Growth rates (s^{-1}) from the full linear model as a function of vertical wavelength and azimuthal wavenumber for various swirl ratios. The axisymmetric model used a mixing coefficient of $K = 6.0$ cm^2 s^{-1}, and the linear model used a mixing coefficient of $K_p = 6.0$ cm^2 s^{-1}. A growth rate of zero means that the disturbance was not growing or was damped. The dots denote points where the linear calculations were made and are useful in locating azimuthal wavenumber on the diagrams, since the calculations were made only at integer wavenumbers.

At $S = 0.8$, wave 1 is stable, and only wave 2 is unstable. By $S = 1.0$, wave 2 is still most unstable; however, a second region of instability has appeared at a vertical wavelength of ~125 cm and an azimuthal wavenumber of 3 or 4. As pointed out above, the second region of instability represents a different mode. As S is further increased, the unstable region for the second mode expands toward longer vertical wavelengths, and by $S = 1.4$ it occupies most of the diagram (except for wave 2 near vertical wavelength 500 cm, which is still mode 1) and is most unstable for wave 4 and a vertical wavelength of 200 cm. At $S = 2.0$, wave 4 is still most unstable but the vertical wavelength has increased. By $S = 2.8$, the most unstable wave is switching to 5, and at $S = 3.5$ and 4.5, wave 5 is most unstable, and the vertical wavelength continues to increase with increasing S. Note also that at $S = 4.5$, the growth rates have become quite large with e-folding times of ~0.1 s.

We will show later that at swirl ratios larger than 4, the nondivergent barotropic model gives an adequate estimate of the growth-rate spectrum (at infinite vertical wavelength of course). Thus for swirl ratios higher than 4.5, we continued the analysis with the nondivergent model and found that at $S = 10.0$, the wavenumber of maximum instability switched to 6. At that swirl ratio, however, the radius of the maximum tangential velocity in the axisymmetric model is very near the edge of the updraft hole and the assumptions leading to the axisymmetric model are probably breaking down.

5. The wave structure

In the previous sections, we pointed out that there are two separate modes of instability: one (mode 1) that appears at low swirl ratio and low azimuthal wavenumber, and a second (mode 2) that appears at moderate swirl ratio ($S \approx 1.4$) and somewhat larger azimuthal wavenumber. Figs. 6–8 show the structure of the *most unstable* wave at $S = 0.6$ (wave 1), $S = 0.8$ (wave 2) and $S = 1.4$ (wave 4). In each of these figures, there are two rings, the inner one indicating the radius of maximum vertical and azimuthal vorticity (they are always at the same radius), and the other the radius of maximum azimuthal wind of the basic state. Waves 1 and 2 represent mode 1, while wave 4 is an example of mode 2. In all three waves, the rotational part of the horizontal wind dominates the divergent part (by a factor of 10). Thus the streamfunction determines the horizontal wind.

For mode 1 (waves 1 and 2), the maximum amplitude of the streamfunction is *inside* the vorticity maximum of the basic state. The perturbation vertical vorticity field consists of strong maxima and minima inside the vorticity maximum of the basic state, with

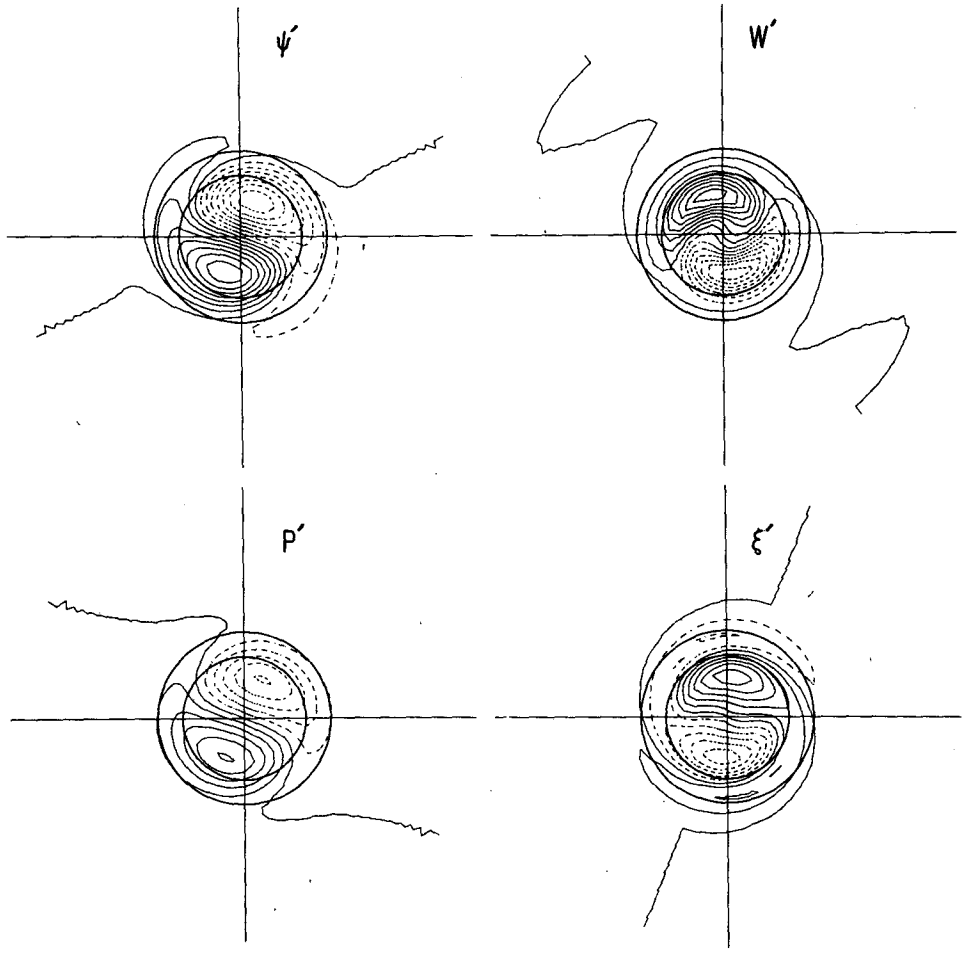

FIG. 6. Distribution of perturbation streamfunction ψ', vertical velocity W', pressure P' and vertical vorticity ξ' on an arbitrary horizontal plane through the center of the basic vortex for azimuthal wavenumber 1 with a vertical wavelength of 400 cm. The swirl ratio of the basic state was $S = 0.6$. The inner rings on the diagram denote the radius of maximum vertical vorticity of the basic state, and the outer rings denote the radius of maximum axisymmetric tangential velocity. The end of the zero contours defines r_0. The phase of ξ' was set equal to a constant in the computer graphics beyond a certain radius to simplify the figure.

weak secondary perturbation vorticity maxima and minima outside this ring. Most of the perturbation amplitude of the fields shown is contained inside the ring of maximum tangential velocity of the basic state.

In contrast to mode 1, the streamfunction amplitude of mode 2 (wave 4) is a maximum *outside* the ring of maximum basic state vorticity with a weak secondary maximum inside this ring. There are now strong maxima and minima of perturbation vertical vorticity outside this ring, as well as inside. Finally the perturbations have considerable amplitude outside the ring of maximum tangential velocity of the basic state.

Except for wave 1, where there can be, and is, flow across the center of the basic vortex, the perturbation velocities are very low near the center of the basic vortex. As S increases the center of action of the unstable waves moves outward as the annular ring of vorticity of basic state expands.

Finally, the streamfunction structure shown in these figures compares very closely with the streamfunction structure of the same waves computed by the nondivergent barotropic model described earlier. That is, wave 2 at low values of S in the barotropic model is similar in structure to wave 2 in the full model, where the streamfunction amplitude is maximum inside the ring of maximum basic-state vorticity, i.e., wave 2 in both models at low S corresponds to mode 1 of the full model. At larger values of S, all waves in the nondivergent model correspond to mode 2 of the full model, where the maximum amplitude of streamfunction is outside this ring. The sudden transition from wave 2 being most unstable

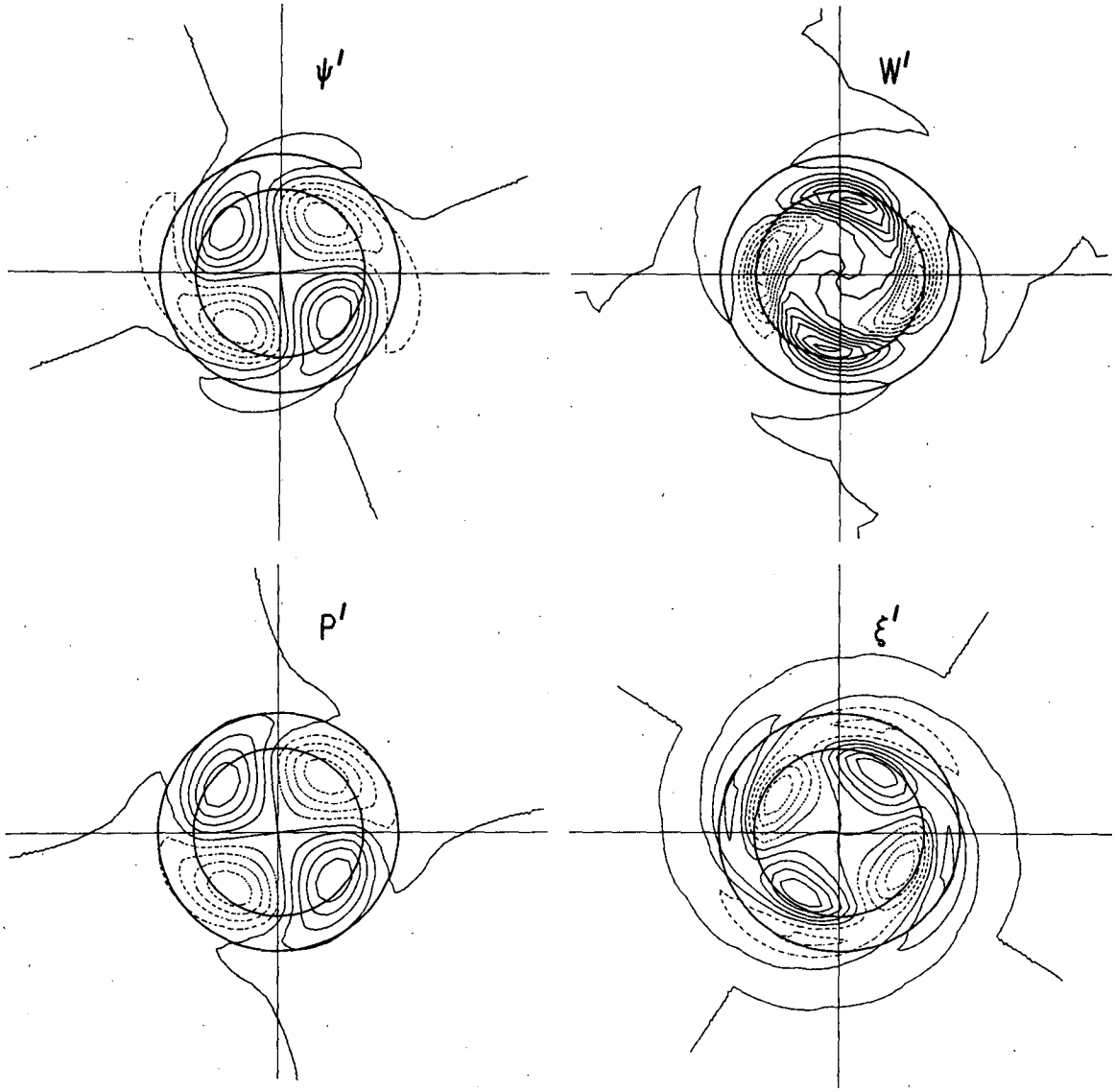

FIG. 7. As in Fig. 5 but for azimuthal wavenumber 2, vertical wavelength 400 cm, and a swirl ratio of $S = 0.8$.

to wave 4 in Fig. 4 is, as with the nondivergent model, due to the rapid increase with S of the growth rate of this second mode.

6. Wave energetics

The kinetic energy equation for the perturbations in this problem is

$$\frac{\partial K_e}{\partial T} = -\overline{V'_\theta V'_r\left(\frac{\partial V_\theta}{\partial r} - \frac{\bar{V}_\theta}{r}\right)}^{v} - \overline{V'_r W' \frac{\partial \bar{W}}{\partial r}}^{v} + \text{Disp}, \quad (11)$$

where the overbar with a subscript v denotes an average over the volume of the wave, K_e is the volume integrated kinetic energy, and Disp denotes frictional dissipation. The first term represents sources of energy from the radial shear of the tangential wind, and the second represents energy sources from the radial shear of the vertical wind. For comparison the energy equation when the waves are assumed to be vertically invariant and governed by the nondivergent barotropic vorticity equation is

$$\frac{\partial K_e}{\partial T} = -\overline{V'_{\theta_\psi} V'_{r_\psi}\left(\frac{\partial \bar{V}_\theta}{\partial r} - \frac{\bar{V}_\theta}{r}\right)}^{v}, \quad (12)$$

where the subscript ψ denotes the rotational part of the wind.

Fig. 9 shows the three terms on the right-hand side of Eq. (11) for wave 2 with a vertical wavelength of 400 cm (nearly the most unstable vertical wavelength at all swirl ratios). In order to demonstrate the relative importance of the nondivergent barotropic energy

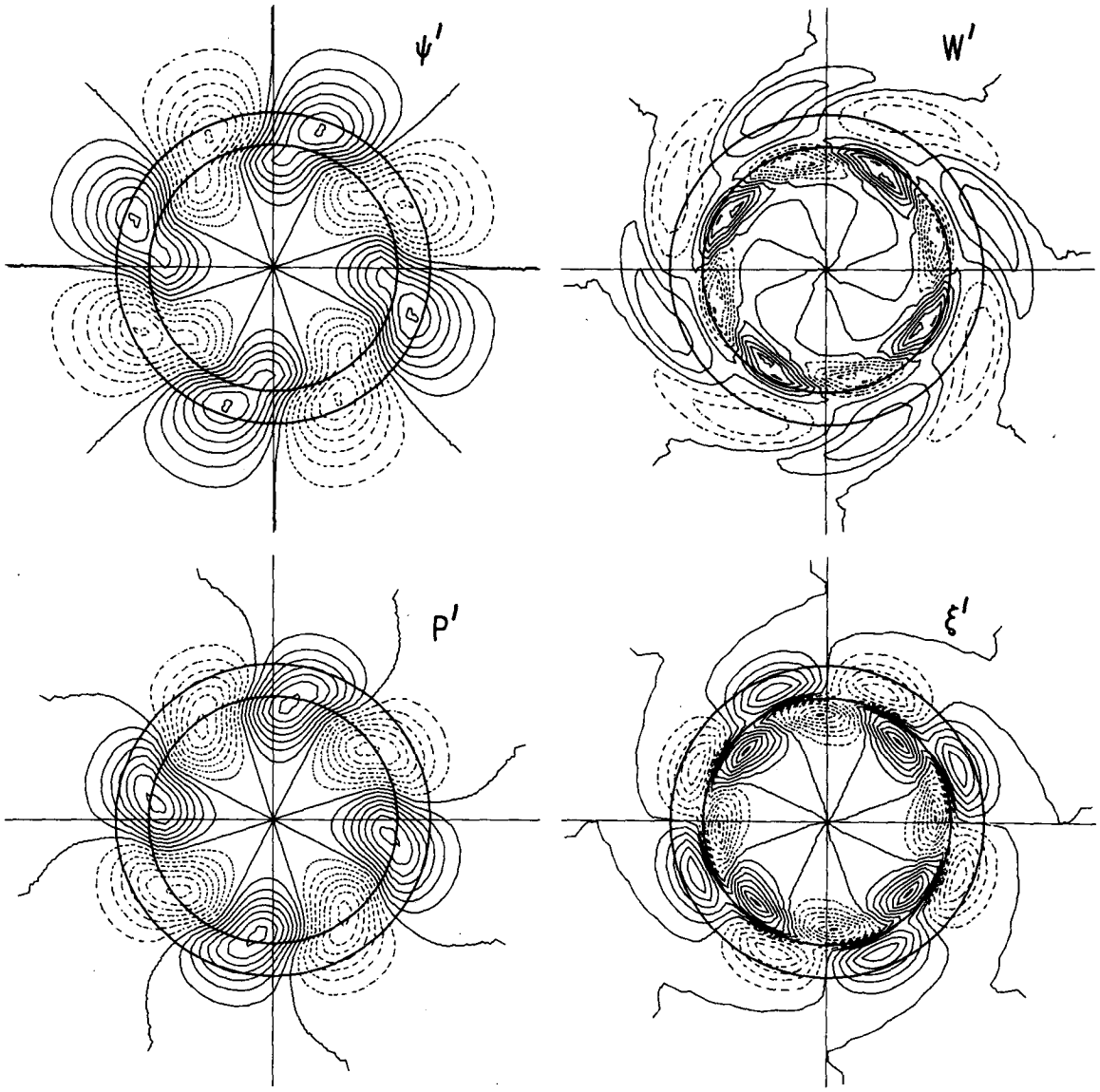

FIG. 8. As in Fig. 5 but for azimuthal wavenumber 4, vertical wavelength 200 cm, and swirl ratio $S = 1.4$.

source, both the term on the right side of (12) and the negative of the difference between this term and the first term on the right-hand side of (11) are plotted. This latter quantity is referred to as Div in the figure, since it arises from the divergent part of the horizontal wind. For convenience we will refer to the former as the nondivergent barotropic energy source.

Note that a change in wave structure of wave 2 as the swirl ratio increases is clearly indicated in the energetics. At low swirl ratio, the energy of wave 2 is being derived from the radial shear of the vertical wind, while that coming from the radial shear of the tangential wind is negligible. As S is increased, the nondivergent barotropic energy source increases linearly, while the source from the vertical wind decreases. Note also that the source from the Div is negative, but small for all S. At $S = 1.6$ the nondivergent barotropic source and the source from the vertical wind are equal, and at high S almost all the energy comes from the nondivergent barotropic term. Thus, at large S the nondivergent barotropic model would give an accurate estimate of the stability of the basic state. In fact, the contribution to the growth rate from the nondivergent barotropic term in the full model is nearly identical to the growth rate calculated with the nondivergent barotropic model (see Fig. 3). Thus, at large S the radial shear of the vertical wind does not significantly alter the structure of the wave from that of the nondivergent barotropic model. Its main effect is to cause the waves to spiral upward.

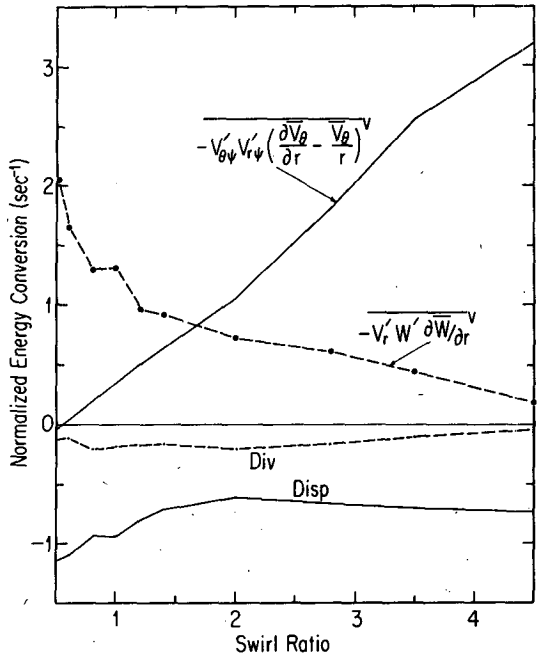

FIG. 9. Components of the energy budget [Eq. (11)] for wave 2, vertical wavelength 400 cm, as a function of swirl ratio. These terms have been normalized by twice the kinetic energy of the wave to give their contributions to the growth rate. The first term on the right of (11) has been partitioned into the term on the right of (12) plus a remainder, which is denoted as Div.

Fig. 10 shows the energy budget for wave 4 at the most unstable vertical wavelength as a function of S. As with wave 2, the energy source from the vertical wind is important at low values of S, but now it is about the same magnitude as the nondivergent barotropic term. Furthermore, the nondivergent barotropic term grows even more rapidly with S than it does with wave 2, so that by $S = 4.5$ it essentially determines the growth rate.

It is perhaps not surprising that the nondivergent barotropic term dominates the energy conversion at large S, since the vertical component of vorticity is much larger than the azimuthal component. This in turn is also easily explained. The azimuthal vorticity is due to the radial shear of the vertical wind. The maximum magnitude of the vertical velocity is essentially determined by the volume flow rate through the chamber. If, as is usually done, the swirl ratio is varied by fixing the volume flow rate and varying the rotation of the air entering the chamber, the maximum magnitude of the vertical velocity will be only a slow function of S (see Fig. 4 of G). This then puts an upper bound on $\partial\bar{W}/\partial r$, and hence the azimuthal vorticity, since the width of the shear zone is independent of S. Thus the azimuthal vorticity should be at most a slow function of S. The average vertical vorticity of the system, on the other hand, increases with increasing rotation rate of the screen. Hence with increasing S, the vertical vorticity will gradually dominate the azimuthal vorticity. Fig. 11 is a plot of the maximum magnitude of the vertical and azimuthal vorticity as a function of S in the axisymmetric model with $K = 6$. This figure clearly shows how the vertical vorticity increases more rapidly than the azimuthal vorticity as S becomes large. At near zero S, there is little azimuthal vorticity and the vertical vorticity is confined to a small region at the center. With slight increases in S, $\bar{W}$ along the axis is reduced, implying the development of increasingly negative azimuthal vorticity near the center. When the downdraft in $\bar{W}$ appears at the center (at $S = 0.45$), the maximum magnitude of the vertical vorticity decreases rapidly with S as this vorticity is swept into the annular ring at some distance from the center. After the downdraft is established, the azimuthal vorticity is essentially constant, while the vertical vorticity increases rapidly. Since the vertical vorticity is much larger than the azimuthal vorticity at large S, the energy source from the radial shear of the tangential wind dominates the energy source from the vertical wind at those values of S.

The energetics of wave 2 at low S and wave 4 at moderate and high S clearly show a basic difference in the two modes of instability that were discussed earlier. Mode 1 was the most unstable mode at low S and was limited to azimuthal wavenumbers 1 and 2. The energy budget for wave 2 at low S (the budget

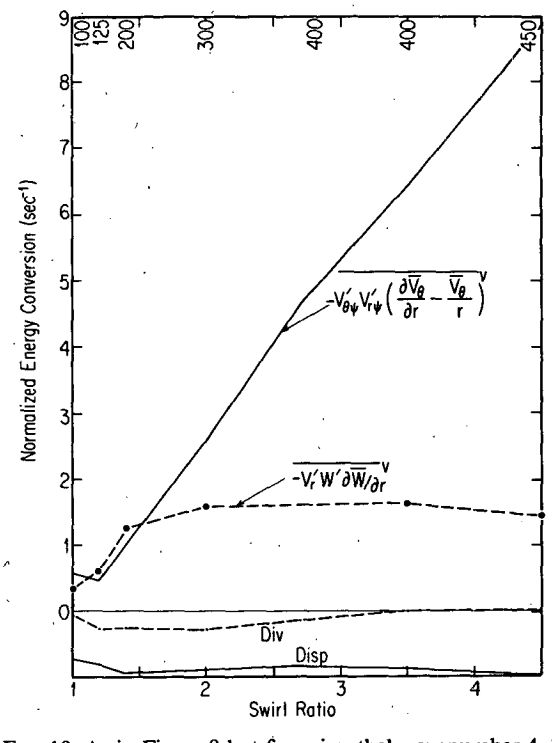

FIG. 10. As in Figure 8 but for azimuthal wavenumber 4. The most unstable vertical wavelength was used at each swirl ratio. The vertical wavelength (cm) used is shown across the top of the figure.

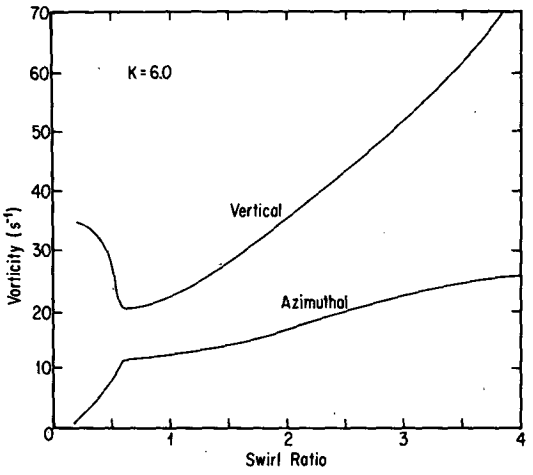

FIG. 11. Vertical and azimuthal vorticity in the axisymmetry as a function of swirl ratio. The axisymmetric model used a mixing coefficient $K = 6.0$ cm^2 s^{-1}.

for wave 1 was similar) shows that this mode receives most of its energy from the radial shear of the vertical wind. Note, however, that mode 1 also appears in the barotropic model, where there is no energy source from the vertical wind. Thus it cannot be said that mode 1 owes its existence to the radial shear of the vertical wind. Mode 2, on the other hand, was most unstable at the higher azimuthal wavenumbers and appeared at $S > 1.0$. In this mode, the nondivergent barotropic energy source plays an important role at low S, and at high S it completely dominates the energy budget. Thus it could be said that mode 2 receives most of its energy from the radial shear of the tangential wind.

As S increases, wave 2 takes on the appearance of mode 2. Fig. 9, however, shows that this transition is gradual as the vertical vorticity increases relative to the azimuthal vorticity.

Finally, the reason why the vertical wavelength increases with increasing S is revealed by their energy budgets. Since the nondivergent barotropic energy source clearly increases with increasing S relative to all other energy sources, at some point the wave must be considered essentially governed by the nondivergent barotropic equations. In such a system, the vertical wavelengths are infinite. Thus, as the nondivergent barotropic source generally dominates the energy budget, there should be a tendency for the vertical wavelength to increase.

7. The predicted transitions

Fig. 12 displays the information given in Fig. 4 in a more concise form. It shows the growth rate of the most unstable vertical wavelength as a function of azimuthal wavenumber and swirl ratio. This figure is presented in part for comparison of the full model results with the upper panel of Fig. 3, which shows the results from the nondivergent model. Note that the two figures are similar, especially at high swirl ratio. One difference is that the maximum growth rates at a particular swirl ratio are more sharply peaked at a particular wavenumber in the full model. This is most likely due to the inclusion of eddy viscosity in the full model, which will affect the growth

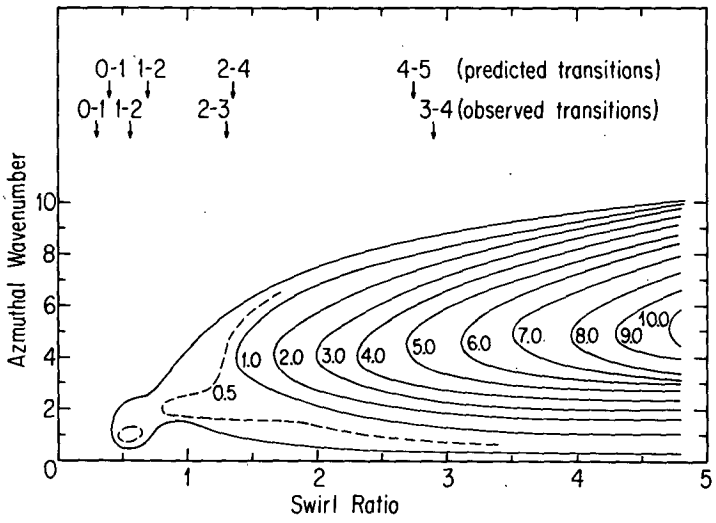

FIG. 12. Growth rates (s^{-1}) of the most unstable vertical wavelength as a function of azimuthal wavenumber and swirl ratio from the full model. The axisymmetric model used a mixing coefficient of $K = 6$ cm^2 s^{-1}, and the linear model used $K_p = 6$ cm^2 s^{-1}. The arrows across the top denote the swirl ratio of the observed and predicted transitions. (See the text for further explanation.)

rate of the higher wavenumbers more than the lower wavenumbers and implies that transitions from one wavenumber being most unstable to another are more clearly defined. A second difference is that wavenumber 1 is unstable, while in the nondivergent model it is not.

In Fig. 12 the swirl ratio where the number of secondary vortices in the machine changes is indicated by a series of arrows. For example, 2–3 indicates that, at that value of S, there is a transition from 2 to 3 vortices. The 0–1 transition indicates the transition from an obviously axisymmetric vortex to one where the still single vortex takes on a spiral form. Above this line of arrows is a second set which indicates the swirl ratios where the most unstable mode given by the full linear model changes. Thus 4–5 indicates that the most unstable mode changes from azimuthal wave 4 to azimuthal wave 5. The transition 0–1 indicates the transition from the basic state being stable to one where wave 1 is most unstable. If we can assume that the most unstable wave would be the one that dominates the eddies when they are large amplitude, then this line gives the transitions in the number of vortices as predicted by our linear model for the tornado simulator.

Generally the swirl ratio of the predicted transitions agrees well with the observed transitions. We hasten to point out, however, that this is partially due to our ability to "tune" the model with the eddy viscosity coefficients, as was discussed in Sections 2 and 4. However, notice that the predicted transitions skip a wavenumber. Near $S = 1.2$, the observed transition is from 2–3, while the predicted transition is 2–4. This jump in the predicted number of vortices is probably because of the switch of the most unstable mode from mode 1 to mode 2. Mode 1 is centered inside the basic state vorticity maximum, while mode 2 is centered outside of it. Thus, since the radial width of both modes is similar, for any given swirl ratio the most unstable azimuthal wavenumber of mode 1 might be expected to be less than the most unstable wavenumber of mode 2, for reasons that were discussed in Section 2. As the swirl ratio increases, the radius of the basic state vorticity maximum increases gradually; thus we might expect a gradual increase in the most unstable wavenumber if the radius where these disturbances are centered also increases gradually. However, the change from mode 1 to mode 2 being most unstable represents an abrupt increase in the radius where the disturbances are centered, and therefore an abrupt increase in the most unstable wavenumber is likely.

We are not surprised that the combination of our axisymmetric model and linear model failed to completely predict the observed transitions beyond the swirl ratio where the basic vortex first becomes unstable, since there the axisymmetric model no longer provides an adequate representation of the basic state. This is because at the transition to a higher number of secondary vortices, the next lower number of secondary vortices is already present. These vortices, of course, modify the basic state from that which a purely axisymmetric model would provide.

It was thought at one point that the effect of the unstable wave could be included in the axisymmetric model merely by increasing the eddy viscosity coefficient; after all, these vortices represent unresolved eddies. If this were true, then the effect of the secondary vortices on the basic vortex would be simply to widen the annulus of vertical vorticity, while preserving the radius of its maximum. The effect of this on the growth rate spectrum was explored in Section 2.

However, Fig. 13 clearly shows that a simple increase in the value of K in the axisymmetric model will not simulate the effect of the secondary vortices. In that figure, traces of the radial distribution of vorticity and divergence (in arbitrary units) in the axisymmetric model for $K = 6$ and $S = 0.8$ are shown. Superimposed on these are normalized plots of the tendency due to friction in the axisymmetric model. These latter curves demonstrate the tendency for friction to smooth out the vorticity and divergence profiles, yet leave unchanged the radius of the maximum. (In the case of divergence, the radius of maximum azimuthal vorticity remains unchanged.)

Also included in Fig. 13 is the tendency of the basic state vorticity and divergence due to convergence of the momentum fluxes forced by the unstable eddies. The equations for these tendencies are:

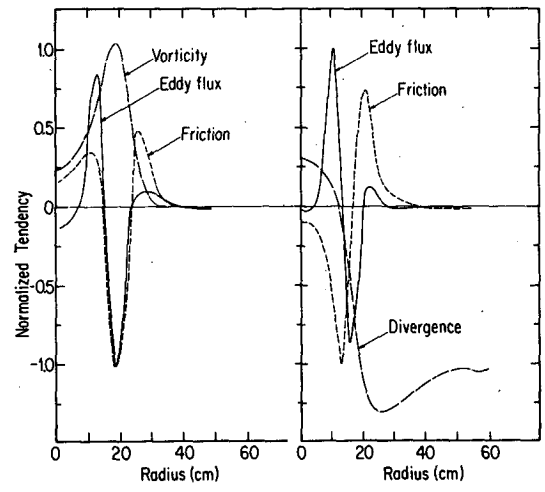

FIG. 13. The radial distribution of the contribution to the tendencies of vorticity and divergence of the diffusion term in the axisymmetric model compared with the radial distribution of the contribution to these tendencies that would be produced by eddy fluxes of the most unstable wave. This diagram is for wavenumber 2, vertical wavelength 400 cm at a swirl ratio of 0.8. Also shown are the radial distributions of vorticity and divergence from the axisymmetric model. All units are arbitrary.

$$\frac{\partial \bar{\xi}}{\partial t} = -\overline{\frac{1}{r}\frac{\partial}{\partial r}(\xi' V_r' r)}^{z\theta} + \overline{\frac{1}{r}\frac{\partial}{\partial r}(\delta' V_\theta' r)}^{z\theta}, \quad (13)$$

$$\frac{\partial \bar{\delta}}{\partial t} = -\overline{\frac{1}{r}\frac{\partial}{\partial r}[\delta' V_r' r]}^{z\theta}, \quad (14)$$

where the overbar again denotes the basic state and the subscript $z\theta$ denotes averages in the θ and z directions. In Eq. (13), the second term on the right tends to be quite small in the unstable waves studied here. Notice from Fig. 13 that the eddy fluxes (which are inward) will tend to move the radius of the maximum magnitude of the two basic state vorticities (vertical and azimuthal) inward. Thus the changes forced by the unstable eddies will be quite different than those forced by the conventional turbulent eddies. In particular, the radius of maximum vorticity in the basic state will not expand as rapidly with S when the secondary vorticities are included in the axisymmetric model as when they are not. Perhaps this less rapid increase in the radius will allow for the appearance of wave 3 at $S = 1.4$, rather than the transition directly from 2–4 that is predicted here. This question can only be explored with an axisymmetric model that allows for an interaction between the unstable eddies and the basic state. Such a model is currently under construction.

8. Conclusion

The rather simple set of calculations presented here demonstrates that the multiple-vortex phenomenon could be a result of the horizontal wind shears that develop in a vortex at high swirl ratio. The models predict there to be transitions from one multiplicity of secondary vortices to another, as observed, at about the observed swirl ratio, and the structure of the waves is at least qualitatively like the observed vortices. The vertical wavelengths predicted by this model are perhaps somewhat longer than observed; however, one must keep in mind that this model assumes a basic vortex of infinite length, while the vertical extent of the vortex in the simulator is limited. The upper and lower boundaries must influence these vertical wavelengths.

The fact that the vertical wavelengths are not infinite shows that these linear waves have a spiral structure. Furthermore, the most unstable waves spiral upward against the rotation of the basic vortex, and the tightness of this spiral decreases with increasing S. These features are observed in multiple vortices that develop in the simulator.

The nondivergent barotropic model gives a good estimate of the growth rate spectrum at high values of swirl ratio, where the vertical vorticity is much larger than the azimuthal vorticity. At low values of S, since the magnitude of the azimuthal vorticity is comparable to the magnitude of the vertical vorticity, the full linear model using the primitive equations is necessary to accurately compute growth rate. However, even at low S the nondivergent barotropic model still provides a crude picture of the stability of the basic vortex. This includes evidence of a different, most unstable mode at low S, as compared to high S.

This study, however, raises several questions. For example, is the wavenumber of maximum instability a function of the radius of maximum vorticity and the width of the annulus of vorticity of the basic state, as we have implied here? This should be fairly easy to show, although we have not done it. If this can be formally shown, then the reason why the number of secondary vortices increases as the swirl ratio increases is easily explained.

The question of why the most unstable perturbation is a different mode at low S as compared to higher S is not answered. This is an important question, since the structure and energetics of these modes are quite different. For example, mode 1 receives most of its energy from the radial shear of the vertical wind, while in mode 2 most of the energy comes from the radial shear of the tangential wind. Whether these properties continue to hold after the unstable waves reach finite amplitude also remains to be seen.

Also, it remains to be shown that the unstable waves will grow large enough that the streamlines will form closed contours away from the center of the basic vortex. If not, then the instability described here cannot account for the presence of the secondary vortices. We suspect that this instability must result in the secondary vortices, since we can think of no other mechanism. However, it may be that the processes that are forcing the basic vortex must be present in order to allow the unstable perturbations to grow large enough. In fact, Rotunno (personal communication, 1982) has already observed this with his three-dimensional model of the tornado simulator. Because of the axisymmetric forcing that continues as the waves grow to large amplitude and the fluxes produced by the eddies themselves, it may be that the structure and perhaps even the wavenumber of the large-amplitude disturbance will differ considerably from the linear disturbance. Models allowing an interaction between the eddies and the basic state will be necessary to answer this question.

Finally, the axisymmetric model described in G either has an updraft everywhere and the maximum tangential wind at a very small radius, or has a downdraft at the center and the maximum tangential winds at relatively large radius. These two situations are observed in the simulator; however, there is also observed to be a transition regime between them, where the maximum tangential wind is at large radius but the flow is upward everywhere, although greatly reduced at the center. In such a system, the vertical vorticity must still be confined to a core of more or

less solid rotation inside the tangential wind maximum and not in an annulus, since a downdraft is necessary to bring the low vorticity into the center. The azimuthal vorticity on the other hand must be in an annular region, since the updraft is observed to be low inside the radius of the tangential wind maximum, rising rapidly to a maximum outside this radius. Thus there is a special set of conditions in the simulator that was not considered here, one where the azimuthal vorticity is contributing to the instability but the vertical vorticity is not. Perhaps this could account for our failure to find wave 3 most unstable.

Acknowledgments. This research was supported by the National Science Foundation under Grants ATM-7920158 and ATM-811554. The final manuscript was edited and prepared by Margaret Sanderson Rae.

REFERENCES

Agee, E. M., J. T. Snow, F. S. Nickerson, P. R. Clare, C. R. Church and L. A. Schaal, 1977: An observational study of the West Lafayette, Indiana, tornado of 20 March 1976. *Mon. Wea. Rev.*, **105,** 893–907.

Brown, J. A., 1969: A numerical investigation of hydrodynamic instability and energy conversions in the quasi-geostrophic atmosphere. Part I. *J. Atmos. Sci.*, **26,** 352–365.

Church, C. R., and J. T. Snow, 1979: The dynamics of natural tornadoes as inferred from laboratory simulations. *J. Rech. Atmos.*, **12,** 111–133.

——, ——, G. L. Baker and E. M. Agee, 1979: Characteristics of tornado-like vortices as a function of swirl ratio: A laboratory investigation. *J. Atmos. Sci.*, **36,** 1755–1776.

Fujita, T. T., 1970: The Lubbock tornadoes: A study in suction spots. *Weatherwise,* **23,** 160–173.

Gall, R. L., 1982: Internal dynamics of tornado-like vortices. *J. Atmos. Sci.*, **39,** 2721–2736.

Haltiner, J. G., and R. T. Williams, 1980: *Numerical Prediction and Dynamics Meteorology.* Wiley, 477 pp (see pp. 75–79).

Kuo, H. L., 1973: Dynamics of quasi-geostrophic flows and instability theory. *Advances in Applied Mathematics,* Vol. 13, Academic Press, 247–330.

Maslowe, S. A., 1974: Instability of rigidly rotating flows to non-axisymmetric disturbances. *J. Fluid Mech.*, **64,** 307–317.

Rayleigh, Lord, 1980: On the stability and instability of certain fluid motions. *Proc. London Math. Soc.*, **11,** 57–70.

Rotunno, R., 1977: Numerical simulation of a laboratory vortex. *J. Atmos. Sci.*, **34,** 1942–1956.

——, 1978: A note on the stability of a cylindrical vortex sheet. *J. Fluid Mech.*, **87,** 761–771.

——, 1982: Numerical simulation of multiple vortices. *Topics in Atmospheric and Oceanic Science: Intense Atmospheric Vortices,* L. Bengtsson and M. J. Lighthill, Eds., Springer-Verlag, 117–215.

Snow, J. T., 1978: On inertial instability as related to the multiple vortex phenomenon. *J. Atmos. Sci.*, **35,** 1660–1677.

Staley, D. O., and R. L. Gall, 1979: Barotropic instability in a tornado vortex. *J. Atmos. Sci.*, **36,** 973–981.

Ward, N. B., 1972: The exploration of certain features of tornado dynamics using a laboratory model. *J. Atmos. Sci.*, **29,** 1194–1204.